SATELLITE REMOTE SENSING APPLIED TO OFF-SHORE WIND ENERGY

Sara Venafra[1], Marco Morelli[2], and Andrea Masini[1]

1. Flyby S.r.l., Livorno, Italy; {sara.venafra / andrea.masini}(at)flyby.it
2. University of Milano, Department of Physics, Milano, Italy; marco.morelli1(at)unimi.it

ABSTRACT

Wind as an energy resource has been increasingly in the focus of attention over the past decades, starting with the global oil crisis in the 1970s. The possibility of expanding wind power production to off-shore locations is attractive, especially in sites where wind levels tend to be higher and more constant.

Wind turbine energy production is usually evaluated by means of a wind turbine power curve, which is provided by the manufacturer and it is an important parameter to estimate wind plant performances. In this study we present a methodology aimed to support both planning of offshore wind farms using historical series of satellite data in order to detect the sites which could provide more wind energy production than others, and near real-time monitoring of offshore wind energy performances by means of SAR data. SAR wind data are retrieved from measured radar backscatter using empirical geophysical model functions, achieving good accuracy, global coverage and greater spatial resolution with respect to other wind measurement methods.

Moreover, we are able to calculate the AC power yield expected behaviour, using detailed models of each part of the wind plants.

In brief, we use SAR data from Cosmo-SkyMed in X-Band and from ERS and ENVISAT in C-Band to generate instant wind speeds and a composite product from NCDC NOAA to investigate wind climatology.

Such methodologies are currently being developed within the scope of SATENERG, a research project funded by ASI (Italian Space Agency). These methods have been applied in several test cases, and successful results in comparison with standard methodologies were obtained.

INTRODUCTION

Wind estimation is very important to support the planning and the monitoring of an off-shore wind farm. The elaboration of SAR imagery to value sea surface wind speed represents an active research field thanks to its global coverage and the high resolution, not currently achievable by other oceanographic remote sensing instrument, such as altimeters and scatterometers. The resolution of scatterometer wind products is 25 or 50 km, while SAR wind estimation is possible at a resolution up to 1 km, making these satellite data very attractive to monitoring coastline windiness.

Several algorithms have been developed in order to retrieve wind fields on the sea surface from SAR products. To date, there are two methods: the first analyses the spectral features of SAR data (1,2) using an empirical linear relation to value wind speed from imagery cut-off frequency, while the second methodology is based on a geophysical model function (*GMF*) for which the normalized radar cross section (*NRCS*) or sigma-naught is expressed as a function of wind field (intensity and direction) and radar incidence angle (3). This last methodology has been originally adopted to data in C-Band (4,5,6) with the development of CMOD4 (7), CMOD5 (8), CMOD-IFR2 (9) and CMOD5.n (10). The model function in C-Band has been extended to X-Band SAR imagery with the implementation of XMOD1 (11), and improved by the development of XMOD2 (12).

With this last newly developed geophysical empirical function XMOD2 (12) the accuracy in wind speed estimation is within 10%, better than the previous wind model XMOD (11). Moreover, with XMOD2 we can retrieve wind speed from Cosmo-SkyMed data in a widened range of wind intensities between 2 and 25 m/s.

The development of wind turbine and inverter models also allow us to estimate the energy production performances of an offshore wind plant: using the SAR wind speed retrieval we calculate instantaneous AC power and by means of an historical series of wind data we detect the areas with major windiness, which is most productive from an energetic point of view.

Further details of adopted methodologies and relative results are described in the next sections.

METHODS

In this section the data and the method adopted to support both planning and monitoring of offshore wind farms are presented.

Description of Instruments

SAR data have been used to retrieve sea surface wind speed: COSMO-SkyMed and ERS 1/2, ENVISAT ASAR in X and C Bands, respectively.

COSMO-SkyMed (Constellation of small Satellites for Mediterranean Basin Observation) satellite constellation (13), was funded by Italian Space Agency (ASI) and conceived as a dual-use system, civilian and defence, for a wide range of applications, such as risk management, scientific and commercial applications, etc. Its first satellite was launched in June 2007. The SAR X-Band has the advantage to operate independently of weather and day night, providing continuous observations of the area of interest. This instrument has different types of acquisition mode, for this study SAR products acquired in DGM (Detected Ground Multi-Look) Stripmap image mode Level 1B were elaborated, with a spatial coverage of about 40×40 km^2, in VV polarization, with an incidence angle between 18° and 45°, and a ground resolution of about 3 m.

ERS 1/2 (European Remote sensing Satellite) and ENVISAT (ENVIronmental SATellite) are C-band SAR and ASAR, respectively, operated by the European Space Agency (ESA), which provided continuous global measurements of the atmosphere, ocean, land, and ice since 1991. For this study ERS SAR PRI (Precision Image) and ENVISAT ASAR Image Mode Precision Image products were used that are multi-look ground range images with a spatial coverage of about 100 km $\times$ 100 km, VV polarization and a ground resolution of 12.5 m.

SAR data need a calibration step (14,15) before their processing to wind, in order to obtain quantitative information independent of the instrument and the embraced assembly line. In fact it is necessary to compensate the range spreading loss, the antenna pattern gain and the incidence angle variations of the received signal. By means of Eq. (1) the SAR COSMO-SkyMed calibration has been carried out.

$$\sigma_0(i,j) = \frac{img(i,j)^2 R_{ref}^{2R_{exp}} \sin(\alpha_{ref})}{F^2 K} \tag{1}$$

where $\sigma_0(i,j)$ represents the *RCS* (Radar Cross Section) corresponding to image position (i,j) on the range and azimuth, respectively, $img(i,j)$ is the value of SAR pixel in Digital Number (DN), R_{ref} is the calibration reference slant range, R_{exp} is the reference slant range exponent, α_{ref} is the calibration reference angle, F is the scaling factor and K is the calibration constant.

In this work we utilize the ESA software NEST (http://envisat.esa.int/nest/) which is able to return the SAR data just calibrated.

The main difference between SAR data in X or C-Band is in the spatial resolution which is better for X-band products than C-band ones, making X-band data more sensitive to sea surface roughness. In consequence the retrieval of sea surface wind speed from X-SAR data is more accurate than that estimated by means of C-SAR products.

Data Space

In order to avoid the ambiguity of 180° due to the impossibility to distinguish upwind from downwind and to associate SAR features to other physical phenomena (not wind) at the same spatial resolution, such as ocean drift systems, wind direction has been introduced externally. This wind direction

is used for the estimation of sea surface wind speed from SAR data. In detail we have used wind direction provided by the NOAA (National Oceanic and Atmospheric Administration) National Climatic Data Center (NCDC), http://www.ncdc.noaa.gov/thredds/dodsC/oceanwinds6hr.html. These marine surface data are observed by research and VOS ships, moored and drifting buoys, and multiple satellites and archived by NCDC as national records. The data are blended together by NOAA with advanced methods to increase resolution and reduce both bias and sampling/analysis errors. The blending also serves as a tool for "data reduction and" and "information deduction". Then the global gridded products are made available via web-based interactive servers, with features of visualization, data manipulation, data sub-setting and downloading in user preferred formats.

These wind data are 6-hourly and 0.25° global sea winds, available since July 1987. Figure 1 shows an example of blended and gridded global wind fields from the multiple satellites on January 15, 2012, 00:00 UTC.
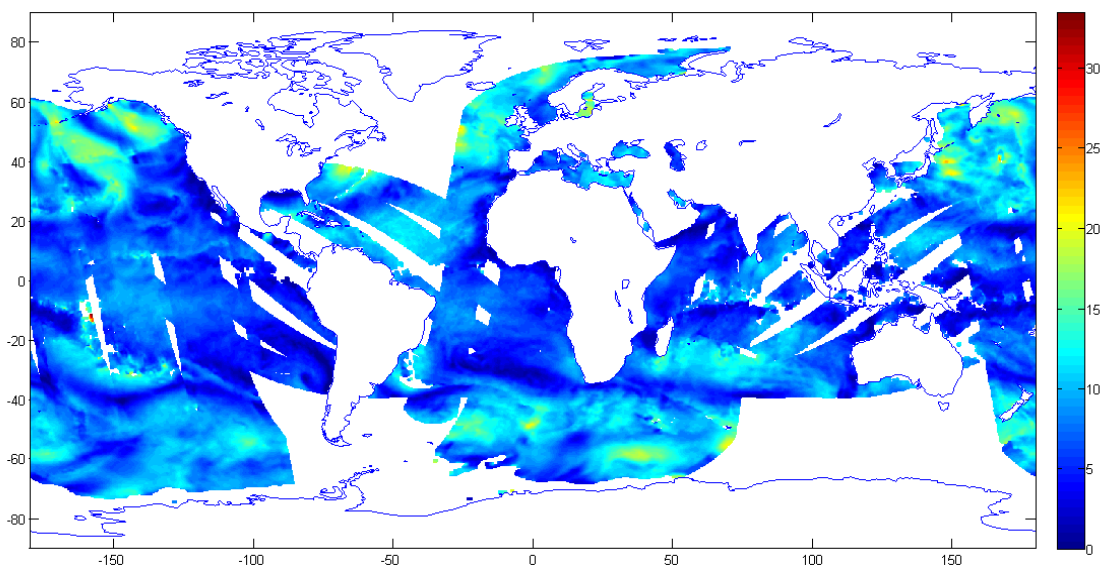

Figure 1: Example of NASA RSS satellite global sea winds on January 15, 2012, 00:00 UTC.

These satellite data were not only used to return wind direction but also to build up a database of historical series of data that, once processed, allows us to identify areas with a major windiness, supporting the design of offshore wind plants. These global sea winds from January 1, 2000 till December 31, 2011 were downloaded, i.e., for a total of twelve years with the aim to acquire information regarding the wind trend which affects the energy production efficiency on several areas with a global coverage.

SAR sea surface wind speed retrieval

The development of a GMF to relate wind field to SAR incidence angle (larger than 20°) is based on the so-called Bragg scattering (16). For this theory the intensity variation in SAR imagery is proportional to the amplitude of sea surface waves. In detail, the waves for which there is a major scattering are those whose wavelength is $\lambda_{Bragg} = \lambda_{Radar}/(2\sin\theta)$ where λ_{Radar} is the radar wavelength and θ is the incidence angle between the radar incident beam and the perpendicular at the incident surface. It describes the interactions between the centimetre radar wavelengths generally used and the ocean surface short gravity waves and capillary waves. The Bragg resonant wavelength depends on the incidence angle; it is larger at steep incidence angles and decreases as the incidence angle increases. Because the ocean wave power spectrum falls off sharply at short wavelengths, the radar return decreases accordingly. The maximum signal is received when the radar points towards the upwind and downwind direction and it is a minimum when the wind blows perpendicularly to the viewing angle (crosswind), as shown in Figure 2.
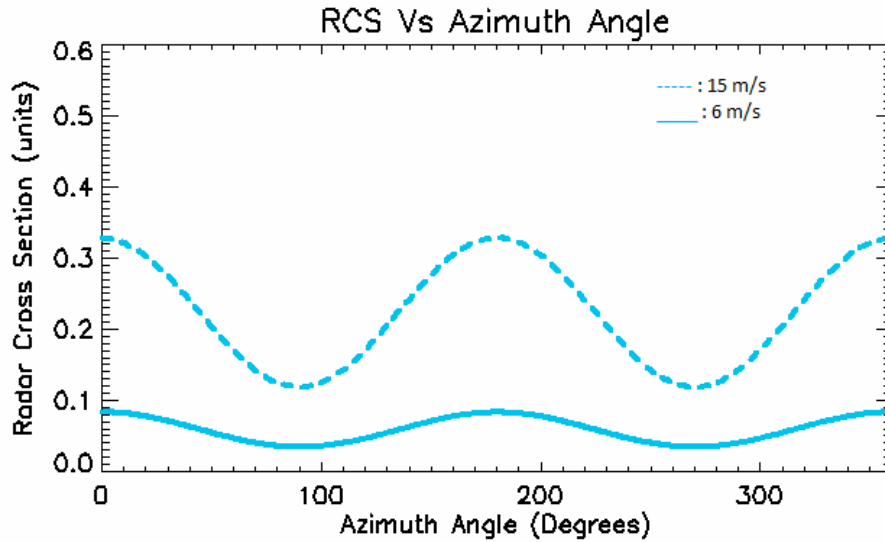
Figure 2: Radar Cross Section versus Azimuth Angle for XMOD2 at incidence angle of 30°.

The model used for the estimation of sea wind speed from COSMO-SkyMed data is that provided by XMOD2 (12) and summarized in Eq. (2). The latter describes the relation between the radar cross section σ_0 and wind field.

$$\sigma_0 = B_0 \left\{ 1 + B_1 \cos(\varphi) + B_2 \cos(2\varphi) \right\} \tag{2}$$

B_0, B_1 and B_2 parameters are functions of wind speed U and incidence angle θ as shown in Eqs. (3-7), while φ is the azimuth angle between the radar look direction and the upwind direction.

$$B_0 = 10^{\beta} U^{\gamma} \tag{3}$$

$$\beta = C(1) + C(2)\theta + C(3)\theta^2 \tag{4}$$

$$\gamma = C(4) + C(5)\theta + C(6)\theta^2 \tag{5}$$

$$B_1 = C(7) + C(8)\theta + C(9)\theta^2 + \left[C(10) + C(11)\theta + C(12)\theta^2 \right] U \tag{6}$$

$$B_2 = C(13) + C(14)\theta + C(15)\theta^2 \left[C(16) + C(17)\theta + C(18)\theta^2 \right] U \tag{7}$$

$C(1)$ - $C(18)$ are 18 coefficients whose values allow us to evaluate SAR wind speed by means of an inversion procedure. Further details about the estimation of these 18 coefficients are described in (7,11,12) both for CMOD4, XMOD and XMOD2, respectively.

The retrieving wind procedure consists of finding the wind speed U which minimizes the following $F(U)$ function:

$$F(U) = \left[M(U, \phi) - \sigma_0 \right]^2 \tag{8}$$

where $M(U, \phi)$ is the radar cross section (RCS) predicted by the wind model used, while σ_0 is that measured on the SAR imagery averaging the calibrated backscatter intensities on 1 km × 1 km sub-images. This box area has been chosen to reduce the radar signal variability due to the "speckle" and the local phenomena especially along the range; in this way the mean difference between the RCS at the scene centre and the borders of the chosen area is within 2%.

The same inversion procedure is used to estimate sea surface wind speed from SAR data in C-Band; in this case using the CMOD4 wind model. Further details about this wind model and its equations are described in (7).

As mentioned in the previous section, we relied on wind direction information gathered from external data, in detail we used NOAA NCDC wind data in order to retrieve wind speed from SAR observations in X and C bands. These wind data have been interpolated both spatially and temporally getting wind data every km and every hour, respectively, with the aim to associate the proper wind direction to the SAR box area of interest for which we want to estimate wind speed.

Estimation of wind turbine energy production

With the aim to support the design and the planning of an off-shore wind plant, the sea global wind fields provided by NOAA NCDC were analysed. In particular, a database of wind fields was built up from January 1, 2000 till December 31, 2011 for a total of twelve years in order to acquire information regarding the wind trend which affects the energy production efficiency on several areas. This database allowed an identification of favourable zones from a wind energy production viewpoint with a spatial resolution of 0.25° and a global coverage.

A database was also created of the wind turbine mostly used for planning offshore plants with different features such as brand, nominal electrical power and hub height. In this way the energy production performances of a chosen wind turbine in a selected area can be simulated.

The energy production of a wind plant is usually carried out with the analysis of the power curve. Defining a model for the electrical power output P_e from a wind turbine is useful in discussing any wind system. We assume that P_e varies as u^K between cut-in and rated wind speeds, u_c and u_R respectively, while k is the Weibull shape parameter. The model wind turbine used for this work is the following (17):

$$
\begin{aligned}
P_e &= 0 & (u < u_c) \\
P_e &= a + bu^k & (u_c \le u \le u_R) \\
P_e &= P_{eR} & (u_R < u \le u_F) \\
P_e &= 0 & (u > u_F)
\end{aligned}
\tag{9}
$$

where u is the wind speed at the hub height, P_{eR} represents the rated electrical power and u_F is the furling wind speed, that is the wind speed at which the turbine is shut down to prevent structural damage. This mathematical model is valid for "pitch controlled" wind systems, in the other cases the electrical power output is not constant beyond the rated wind speed.

The parameters a and b are given by Eqs. (10) and (11):

$$
a = \frac{P_{eR} u_c^k}{u_c^k - u_R^k}
\tag{10}
$$

$$
b = \frac{P_{eR} u_c^k}{u_R^k - u_c^k}
\tag{11}
$$

A typical plot of electrical power output versus wind speed is shown in Figure 3.
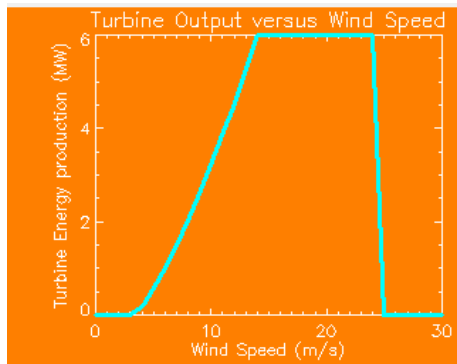

Figure 3: Model wind turbine output versus wind speed, with P_{eR} = 6 MW, u_C = 3 m/s, u_R = 12 m/s, and u_F = 25 m/s.

In this way we calculate the electrical power output P_e from a specific wind turbine varying with wind speed. Using this P_e and by means of Eq. (12) we estimate the yearly power output $P_{e,ave}$ of a wind energy system. $P_{e,ave}$ is the power produced at each wind speed times the fraction of the time at which this wind speed is experienced, integrated over all possible wind speeds. The integral form of $P_{e,ave}$ is:

$$P_{e,ave} = \int_0^\infty P_e f(u) \, du \qquad (12)$$

in which $f(u)$ is the probability density function of wind speeds provided by NOAA NCDC global winds data distribution for the selected year and wind turbine hub height. Wind speed at hub height z is obtained by means of this equation $u = \left(u_{ref} \ln(z/z_0)\right) / \ln(z_{ref}/z_0)$, where u_{ref} is the wind speed at reference height z_{ref} (10 m above sea level in our case) and z_0 is the roughness length typically equal to 0.0002 m at the sea surface (18). This is a logarithmical varying wind profile derived using a mixing length approach and assuming neutral stability conditions, neglecting the effect of differences in atmospheric stability (18).

The so-called Weibull distribution $f(u)$ is typically described by the following equation:

$$f(u) = \frac{k}{c}\left(\frac{u}{c}\right)^{k-1} \exp\left[-\left(\frac{u}{c}\right)^k\right] \qquad (13)$$

where c and k are the Weibull parameters which indicate the *scale parameter*, indicative of windiness of the examined site and the *shape parameter*, indicative of the output power curve versus wind speed, respectively.

Substituting the Eqs. (9) and (13) in Eq. (12) and reducing to the minimum number of terms, the result is:

$$P_{e,ave} = P_{eR}\left\{\frac{\exp\left[-\left(u_c/c\right)^k\right] - \exp\left[-\left(u_R/c\right)^k\right]}{\left(u_R/c\right)^k - \left(u_c/c\right)^k} - \exp\left[-\left(u_F/c\right)^k\right]\right\} \qquad (14)$$

This expression is used to estimate the average power production of a turbine when the wind speed distribution is not known for the area and the time selected. The term inside the braces of Eq. (14) is called capacity factor *CF*, i.e., the ratio between the estimated yearly energy production and the maximum one which can be provided by the chosen wind system. *CF* represents an important design item in addition to the average power. Typical *CF* are included between 20% and 40%.

In order to calculate $P_{e,ave}$ with Eq. (14) the Weibull parameters need to be estimated, whereas P_{eR}, u_R, u_c and u_F are provided by the turbine manufacturer.

There are several methods to estimate the Weibull parameters. One of these methodologies starts with the integration of Eq. (13) to obtain the distribution function $F(u)$ which can be linearized by taking the logarithm. The result is described by the following equation:

$$\ln\left[-\ln\left(1 - F(u)\right)\right] = k \ln u - k \ln c \qquad (15)$$

which is in the form of a straight line *y=ax+b*. Thus the Weibull parameters *k* and *c* are calculated using the NOAA NCDC wind speed distribution $F(u)$ in the selected area from year 2000 till 2011.

We recommend to extract Weibull parameters for months with the aim to obtain information about the windiness in the chosen site with major accuracy. Generally the Weibull prediction is within 20% of the actual value for either wind speed range that is not bad for a data set which is difficult to describe mathematically.

These estimated monthly Weibull parameters can also be used to calculate the instantaneous AC power production from a wind turbine. Using Eq. (13) one obtains the Weibull function for a specific wind speed which can be predicted directly from SAR imagery or provided by other wind data

sources such as anemometers, buoys, etc. Knowing P_e at this wind speed, we extract the instantaneous power production multiplying P_e by the estimated punctual Weibull function.

From NOAA NCDC wind data one can also analyse the wind direction distribution, detecting the most frequent one for which a major output wind power is expected.

RESULTS

XMOD2 has been validated firstly comparing 53 SAR images with winds up to 7 m/s to QuickSCAT wind speeds. QuikSCAT wind estimates collocated with SAR measurements were obtained through an interpolation of the closest QuikSCAT data which have a spatial resolution of 25 km. The time difference between these measures is within one hour. The *RMS* difference between XMOD2 and QuikSCAT wind speeds is 0.8 m/s (12). This comparison is depicted in the following figure.

Figure 4: Scatterplot of QuickSCAT versus XMOD2 wind speeds for speeds lower than 7 m/s.

By contrast, the analysis of winds in the range 7-25 m/s has been conducted using a data set of 121 images, the majority of which were acquired after November 2009, when only GFS (Global Forecast System) data were available. The GFS data acquired before and after the CSK overpass have been interpolated over time and then over space in order to have collocated SAR and GFS wind estimations. In this case, the RMS difference is 2.0 m/s (12), as shown in the scatterplot of Figure 5.
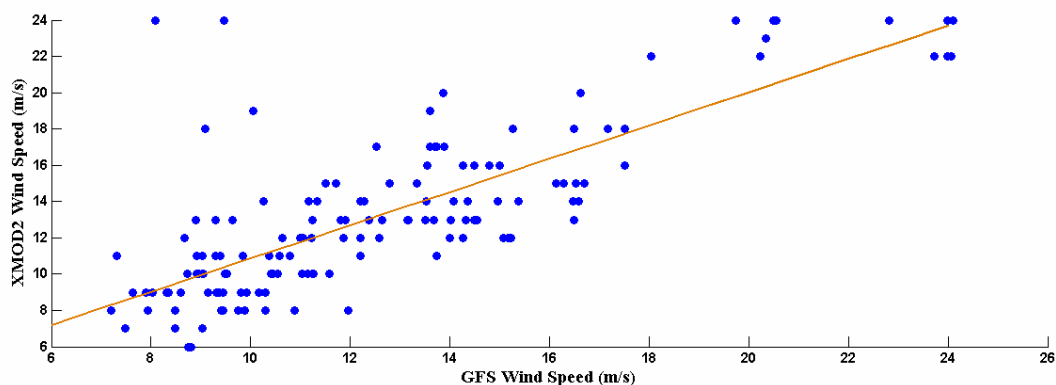

Figure 5: Scatterplot of GFS versus XMOD2 wind speed for speeds in the range 7-25 m/s.

The validation step has also been carried out using 25 Cosmo-SkyMed images acquired between 31/01/2013 and 16/02/2013 and real-time buoy data, accommodating within the retrieval scheme the wind direction provided by the buoys. The maximum time lag between the SAR and buoy data is one hour and the SAR sub-images are exactly collocated with the buoys. The comparison between XMOD2 and buoys winds has returned an RMS difference of about 1.3 m/s (12), as illustrated in the following figure.
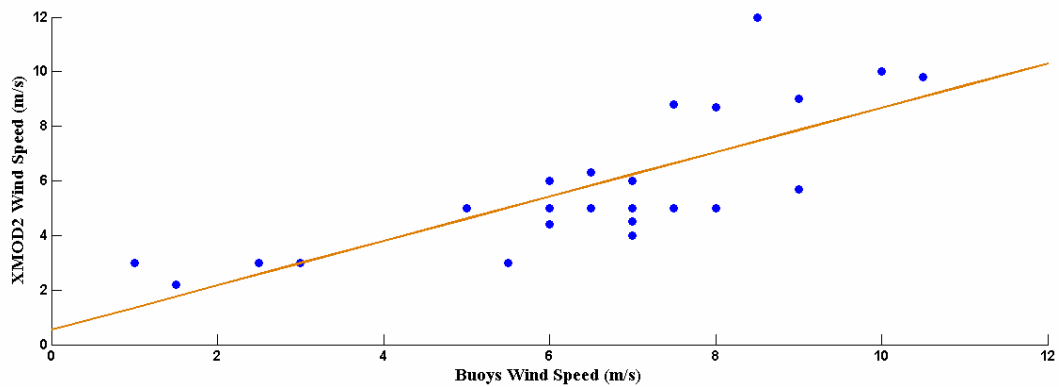
Figure 6: Scatterplot of XMOD2 versus buoy wind speeds.

In Figure 7 two examples of SAR Cosmo-SkyMed wind speed retrieval are illustrated, near the Italian South coasts (a) and in the Norwegian sea (b) with their QuickLooks.
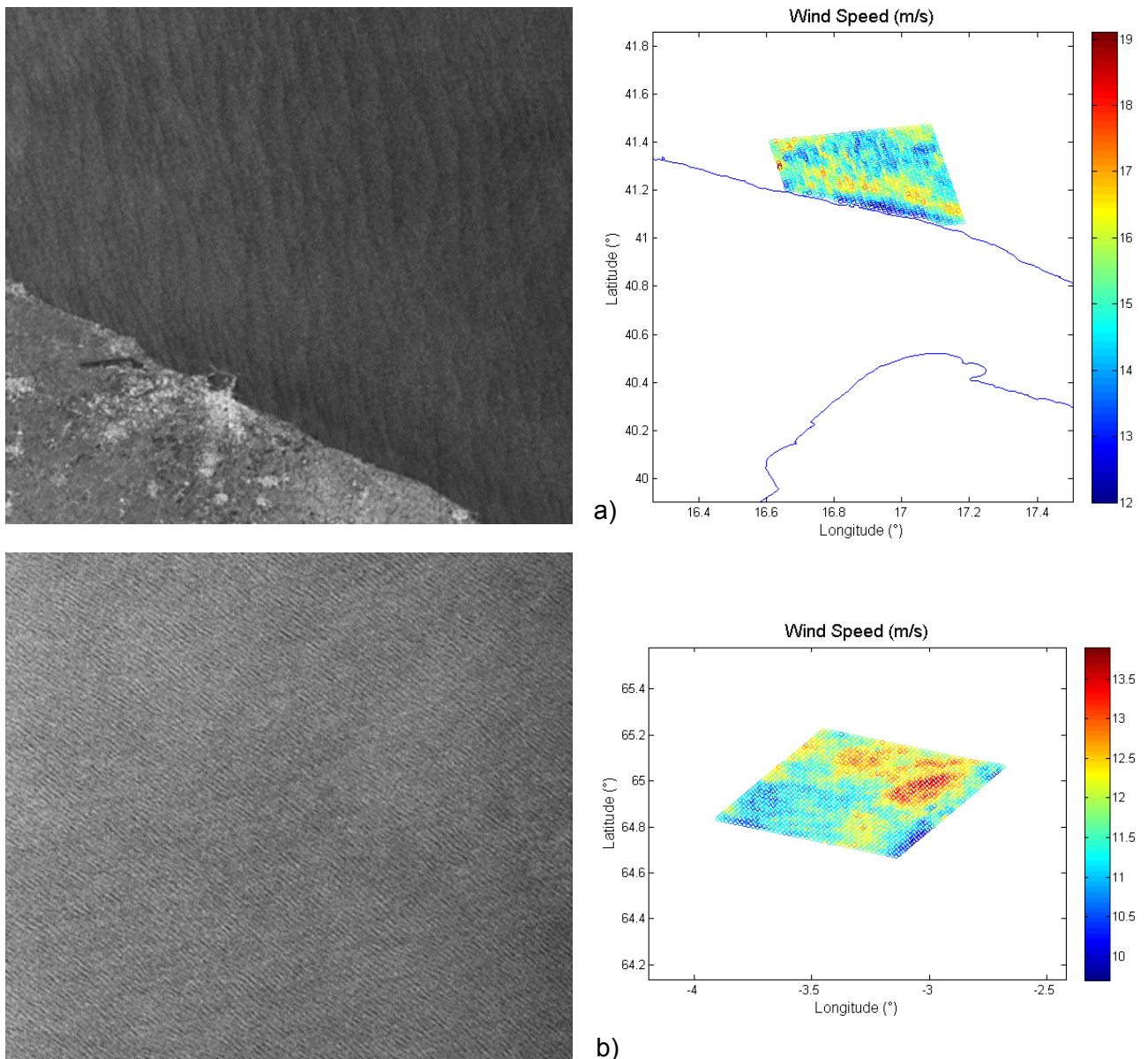

Figure 7: Examples of SAR Cosmo-SkyMed wind speed retrieval and their QuickLooks: near the Italian South coasts (a) and in the Norwegian open sea (b).

Illustrations of SAR C-band wind speed retrieval are depicted in the graph below. Figure 8(a) is obtained from ENVISAT ASAR in the Arabian Sea and (b) represents wind speed retrieved from ERS-2 SAR near the Caribbean coasts.
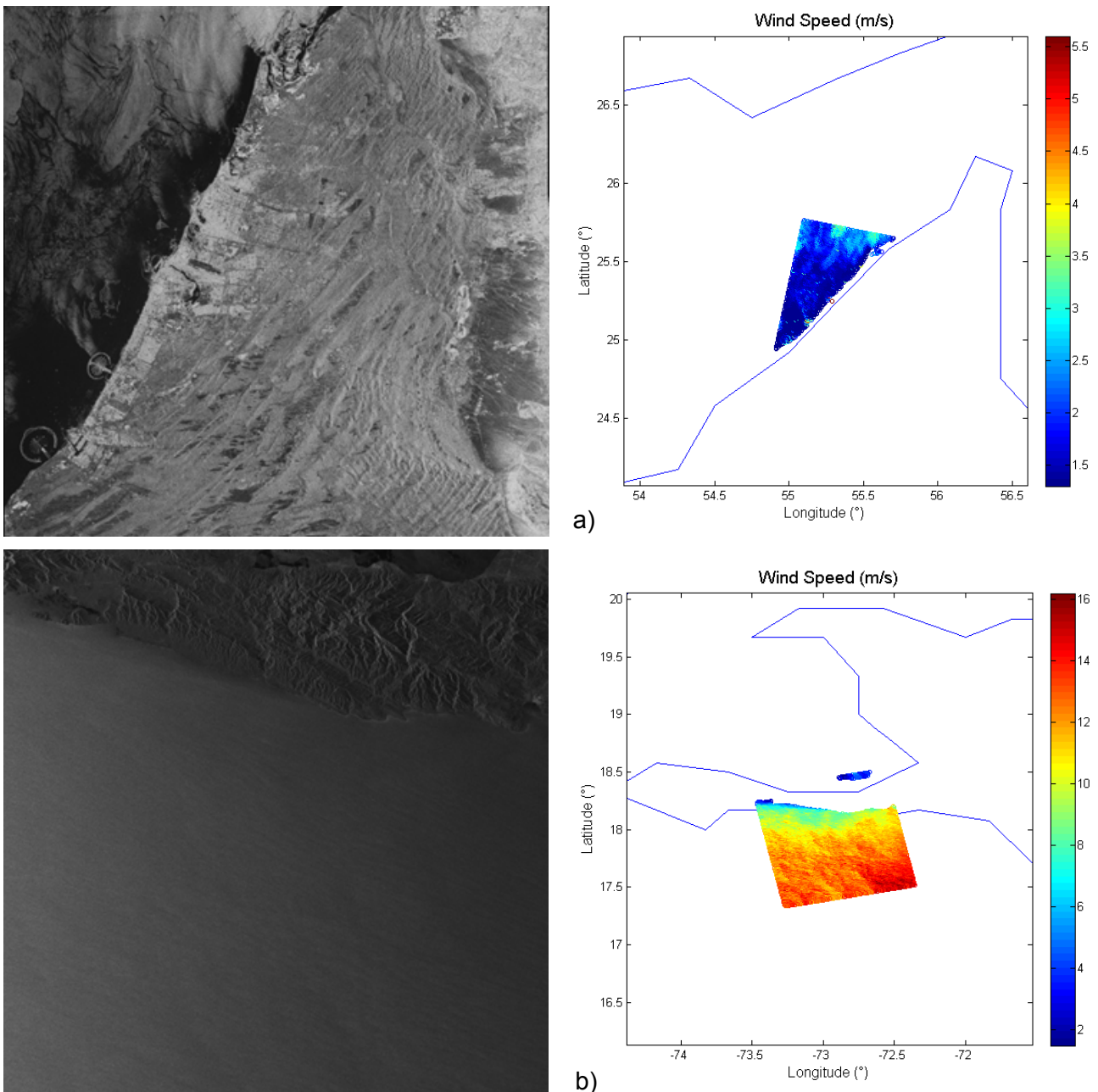

Figure 8: Examples of C-band SAR wind speed retrieval and their QuickLooks: ENVISAT ASAR in the Arabian Sea (a) and ERS-2 SAR near the Caribbean coasts (b).

From Figures 9 to 11 one denotes an example of wind field distribution analysis for a particular site in order to estimate the output energy production power from a possible offshore wind plant installed there. This analysis can be made with a global coverage and a spatial resolution of 0.25°. Using the NCDC NOAA wind data from year 2000 till 2011, we show in Figure 9(a) the wind speed distribution for the site with 18° of longitude and 41° of latitude and the Weibull function estimated for this area (blue curve). Beside this figure, there is the turbine energy production versus wind speed. In this case a Siemens SWT-6.0-154 offshore turbine is considered with P_{eR} = 6 MW, u_C = 3 m/s, u_R = 12 m/s and u_F = 25 m/s and with a hub height of 90 m.

The Weibull fit has provided a square correlation coefficient of about 0.989, a very good result.
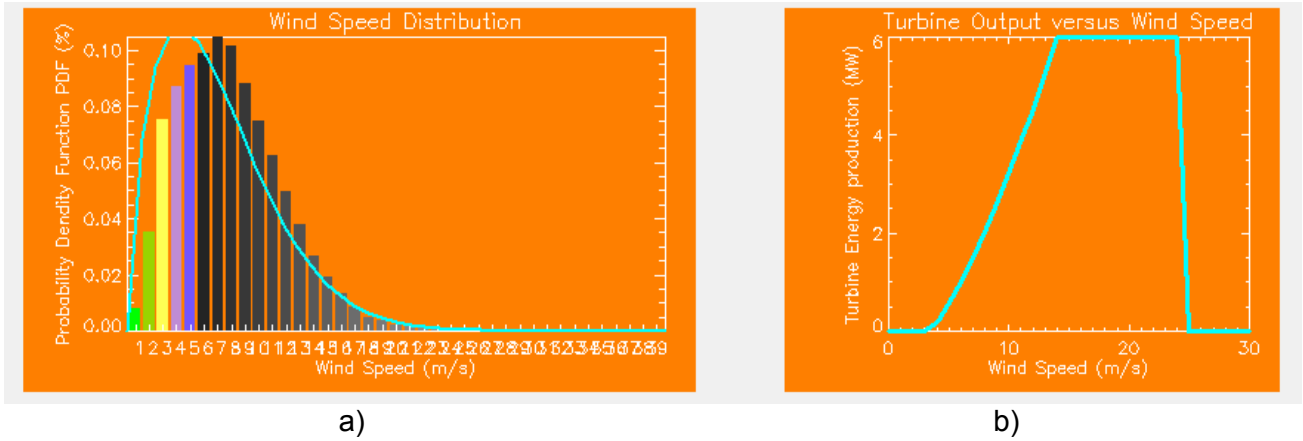
a)   b)

Figure 9: Wind speed distribution at longitude 18° and latitude 42° from year 2000 till 2011 and estimated Weibull function (a); Turbine energy production versus wind speed (b)

The plot of the average power output (see Eq. (12)) for all twelve years versus wind speed and the monthly mean wind speeds for this site are illustrated in Figure 10a and b, respectively.
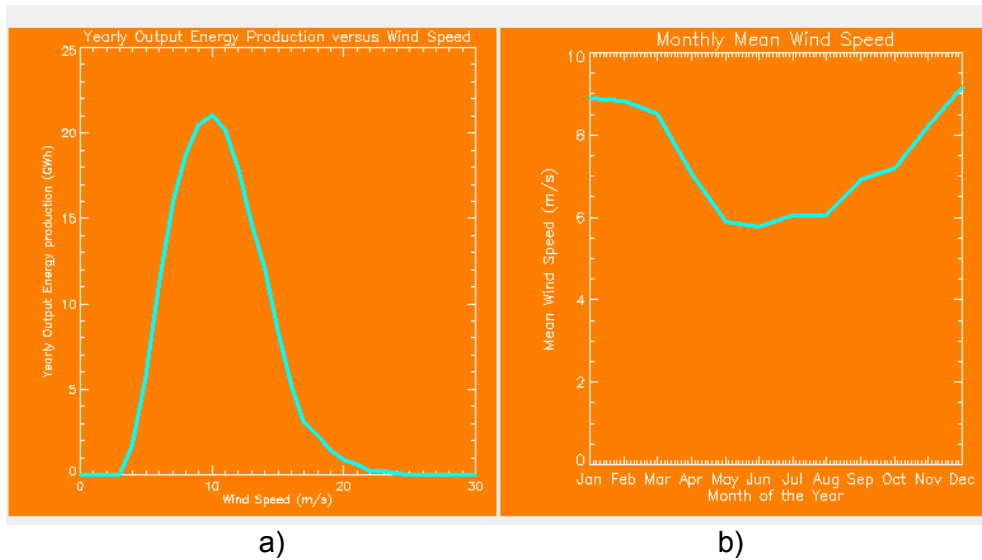

a)   b)

Figure 10: Average power output versus wind speed (a); Monthly wind speed (b)

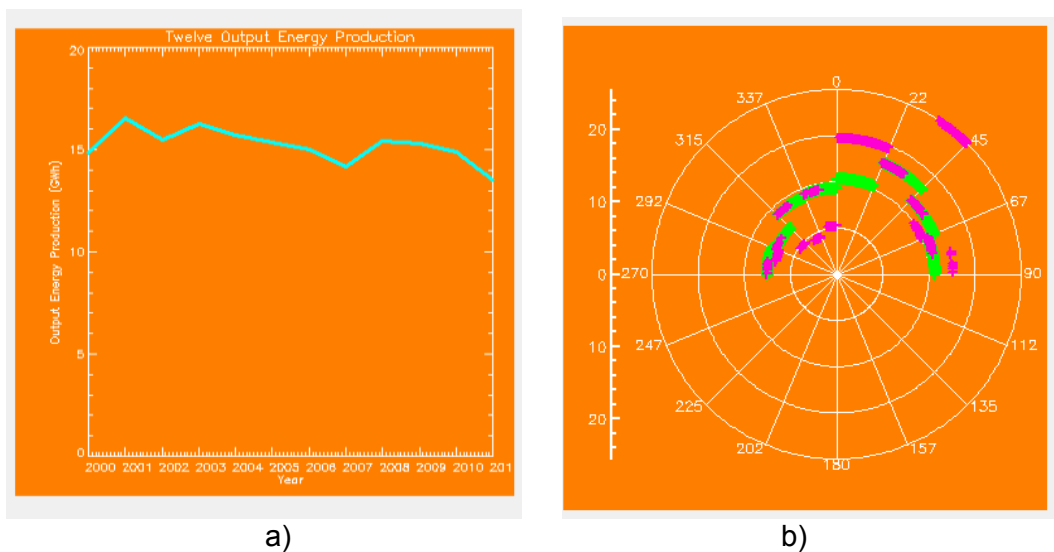a)   b)

Figure 11: $P_{e,ave}$ from January 1, 2000 till December 31, 2011 for the examined site (a); wind direction distribution at major energy production.

Figure 11a shows the retrieved output energy production estimated by means of the twelve years wind distribution provided by NCDC NOAA wind data. With Figure 11a we highlight that every year there is an energy production of about 15 GWh from a single turbine in this area. In Figure 11b a wind rose is depicted, representing the wind direction distribution in green and the wind direction for which there is a major energy production in fuchsia for year 2008 in this case. The most frequent wind direction with a major output energy production (at about 10 m/s as shown in Figure 10a) is between 22° and 45°, as illustrated in Figure 11b.

The capacity factor *CF* for the case study is about 25.3% and the number of equivalent hours is meanly 2300 h/year.

Keeping in mind that the accuracy in SAR wind speed retrieval is within 10%, the accuracy in the estimation output wind energy production will be within 20%, a very good result.

CONCLUSIONS

We have reviewed wind speed retrieval methodologies from SAR imagery with the objective to support the monitoring of the performances of an offshore wind farm with a very high spatial resolution. XMOD2, derived using Cosmo-SkyMed products, has been validated on an extended range of wind speeds between 2 and 25 m/s, returning also a very good agreement with ground truth data. We have also used historical series of satellite wind data in order to support the planning of an off-shore wind plant and to detect the areas with a major estimated energy production. We expect to improve our models in terms of accuracy when a more complete SAR imagery data set becomes available and the wind direction is estimated directly from the SAR data.

ACKNOWLEDGEMENTS

REFERENCES

1   Kerbaol V, B Chapron, T Elfouhaily & R Garello, 1996. Fetch and Wind Dependence of SAR Azimuth Cutoff and Higher Order Statistics in a Mistral Wind Case. International Geoscience and Remote Sensing Symposium IGARSS'96, 21-26 May 1996, Lincoln, Nebraska, USA

2   Kerbaol V, B Chapron & P W Vachon, 1998. Analysis of ERS-1/2 SAR Wave Mode Imagettes. Journal of Geophysical Research., 103(C4): 7833-7846

3   Elachi C (Ed.), 1987. Spaceborne Radar Remote Sensing: Applications and Techniques, pp. 202-204, (New York: IEEE Press)

4   Vachon PW & F W Dobson, 1996. Validation of wind vector retrieval from ERS-1 SAR images over the ocean. The Global Atmosphere and Ocean System, 5: 177-187

5   Zecchetto S, F Nirchio, S Di Tomaso & F De Biasio, 2008. Similarities and differences of SAR derived wind fields using two different methods: the local gradient and the continuous wavelet transform methods. Proceedings of SeaSAR 2008 – The 2nd International Workshop on Advances in SAR Oceanography from ENVISAT and ERS missions, ESA SP-656

6   Zecchetto S & F Di Biasio, 2008. A wavelet based technique for sea wind extraction from SAR images. IEEE Transactions of Geoscience and Remote Sensing, 46(10): 2983-2989

7   Stoffelen A & D Anderson, 1997. Scatterometer data interpretation: Measurement space and inversion. Journal of Atmospheric and Oceanic Technology, 14(6): 1298-1313

8   Hersbach H, 2002. CMOD5; An Improved Geophysical Model Function for ERS C-Band Scatterometry. ECMWF Technical Memoranda, 000, 47 pp. (last date accessed: 29 Jan 2014)

9   Quilfen Y, B Chapron, T Elfouhaily, K Katsaros & J Tournadre, 1988. Observation of tropical cyclones by high-resolution scatterometry. Journal of Geophysical Research, 103: 7767-7786

10   Hersbach H, 2008. CMOD5.N: A C-band geophysical model function for equivalent neutral wind. ECMWF Technical Memoranda, 554, 22 pp. (last date accessed: 29 Jan 2014)

11   Nircho F & S Venafra, 2010. Preliminary model for wind estimation from Cosmo/SkyMed X band SAR data. Proceedings of International Geoscience and Remote Sensing Symposium IGARSS 2010, 25 – 30 July 2010, Honolulu, Hawaii, USA, pp. 3462-3465

12   Nircho F & S Venafra, 2013. XMOD2 - An improved geophysical model function to retrieve sea surface wind fields from Cosmo-SkyMed X-band data. European Journal of Remote Sensing, 46: 583-595

13   COSMO-SkyMed SAR Products Handbook. Document No: ASI-CSM-ENG-RS-092-A (last date accessed: 29 Jan 2014)

14   Laur H, P Bally, P Meadows, J Sanchez, B Schaettler, E Lopinto & D Esteban, 2004. Derivation of the backscattering coefficient in ESA ERS SAR PRI Products. ESA Technical Note ES-TN-RS-PM-HL09, Issue 2, Rev. 5f (last date accessed: 29 Jan 2014)

15   Inversi P, 2009. Cosmo/SkyMed image calibration (e-geos) 3 pp. (last date accessed: 29 Jan 2014)

16   Plant W J, 1990. Bragg scattering of electromagnetic waves from the air/sea interface. In: Surface Waves and Fluxes, G J Geerneart and W J Plant, Editors, Vol. 2 (Kluwer Academic) 41-108

17   Powell W R, 1981. An analytical expression for the average output power of a wind machine. Solar Energy, 26(1): 77-80

18   Peixoto J P & A H Oort, 1992. Physics of Climate (American Institute of Physics & Springer Verlag) 520 pp.